Hindawi
International Journal of Aerospace Engineering
Volume 2021, Article ID 4802182, 12 pages
https://doi.org/10.1155/2021/4802182

Research Article

Numerical Simulation on the Boiling Flow Patterns of Al_2O_3-Water Nanofluid in Micro/Minichannel under Different Hypergravity Levels and Directions

Gen Li and Xiande Fang

Key Laboratory of Aircraft Environment Control and Life Support, MIIT, Nanjing University of Aeronautics and Astronautics, Nanjing, China

Correspondence should be addressed to Gen Li; ligenlglg@163.com

Received 18 August 2021; Revised 29 October 2021; Accepted 18 November 2021; Published 17 December 2021

Academic Editor: Marco Pizzarelli

Due to the influence of hypergravity that has a significant impact on the performance of heat exchanger in aircraft, which is crucial for electronic equipment on the plane and life safeties of pilots and passengers, a numerical study is conducted using Fluent 20R2 software to investigate boiling flow patterns under different gravity levels and directions. In this study, the thermophysical properties of nanofluids are analyzed, and select the most suitable theoretical model of thermal conductivity, viscosity, and surface tension for present simulations. Choose the grid structure of 122,116 after independence check for grid. The VOF approach is employed for present simulation, and the standard $\kappa - \varepsilon$ turbulence model with nonequilibrium wall function is used. The UDFs for mass and energy source terms and thermophysical properties of nanofluid are developed for calculating the HTC of nanofluid. There are three different gravity directions with gravity levels from 1 g to 9 g. The results show that the flow pattern becomes the stratified flow with the gravity levels increasing when the hypergravity direction is perpendicular to the flow direction, and the HTCs decrease with the increment of gravity levels. The vapor-phase transform to circular when the hypergravity direction is the same as the flow direction, and the HTCs of the second half of the tube are decreasing with the increasing gravity levels. On the contrary, the vapor phase is elongated when the hypergravity direction is opposite to the flow direction, and the HTCs show the enhanced tendency.

1. Introduction

With the rapid development of aviation industry, more and more high precision with small volume equipment has been used in modern aircraft, especially heat exchanger, which needs a higher heat transfer efficiency with smaller volume [1–4]. Common liquids such as water, ethylene glycol (EG), and Freon are widely used for heat transfer up to now, while the efficiency of these pure liquids is not high enough in the heat transfer processes. Therefore, many researches have studied the way to improve the liquid's heat transfer efficiency, and the main way is the use of nanoparticles suspended in these fluids, called nanofluids [5–10].

The hypergravity means the acceleration is larger than 1 g (g is the gravitational acceleration, which is approximately equal to 9.8 m/s^2); flight vehicles are usually under hypergravity conditions during takeoff and descent period. For the military aircraft, such as F-35 and Su-57, the gravity level is much higher than the civil aircraft even up to 9 g. Therefore, the performance of heat exchanger under hypergravity condition is vital for electronic equipment on the plane and life safeties of pilots and passengers, and the investigation on the flow boiling characteristics of nanofluids under hypergravity is necessary, consequently. Previous studies in recent years related to the experiment and numerical simulation on the nanofluid flow boiling heat transfer are briefly introduced in the following.

1.1. Experiment on Flow Boiling Heat Transfer of Nanofluids. Sarafraz et al. [11] conducted the experimental research on the flow boiling heat transfer of zirconia–water nanofluid inside an annular heat exchanger with heat fluxes of 10 to 150 kW/m^2, inlet temperatures of 323 K to 353 K, mass flow rates of 1-10 kg/s, and mass concentrations ranging from 0.1 to 0.3%. They found that the concentration of nanoparticle had significant influence on the flow boiling HTC; in other words, the HTC increased with the increment of concentration. They deemed that it was due to the raising of the Brownian motion together with thermophoresis phenomenon, and the enhancement of thermophysical properties was another vital cause for HTC increasing. Using the same experimental apparatus, Goodarzi et al. [12] experimentally investigated the enhancement of graphene oxide nanoplatelets (GONP) for the flow boiling HTC. The base fluids were water-C_6F_{14} and water-n-pentane, and the mass concentration of GONP was 0.1-0.3 wt.%. The results showed that the flow boiling HTC increased with the increasing of the mass concentration of GONP obviously both in water-C_6F_{14} and in water-n-pentane fluid. They considered that the main reason was the increase of the thermal conductivity, thermophoresis, and the Brownian motion of the nanoplatelets which led to the HTC increase. For the above two different base fluids, the maximum enhancement values of HTC were 20-50% and 30-90%, respectively. Dadhich et al. [13] experimentally examined the HTC of TiO_2-water nanofluid in a cement and concrete-based test section with length of 500 mm and ID of 10.7 mm. The volumetric concentration of nanofluid was from 0.05 to 0.2%, and the heat flux, Reynolds number, and pressure were 143 kW/m^2, from 8000 to 24000, and from 1 to 2.5 bar, respectively. According to the experimental results, it was noticed that the HTC of nanofluid was much higher than the water and increased with the enhancement of volumetric concentration.

Using the Al_2O_3 nanoparticles, Mukherjee et al. [14] experimentally analyzed the subcooled flow boiling heat transfer of Al_2O_3-water nanofluid in a horizontal tube with mass concentration of 0.01% to 1%. It was concluded from the experimental results that the HTC of nanofluid was higher than that of pure water and increased with the increment of nanoparticle concentration. Patra et al. [15] experimentally studied heat transfer characteristics of Al_2O_3-water and SiO_2-water nanofluids in a quartz vertical tube with 45 mm ID and 1000 mm length. The volume concentrations were 0.001 vol% and 0.01 vol%. The results exhibited that the HTC was enhanced compared to water, while the enhancement decreased with increasing concentration. It is mainly because of the increasing of thermal resistance caused by excess deposition of nanoparticles on the heating wall when the concentration was high during boiling.

All above experimental investigations on the flow boiling heat transfer characteristics of nanofluids were conducted under normal gravity, and until now, only one literature presented by Dong et al. [1] carried out the boiling heat transfer characteristics of nanofluids under hypergravity condition by using an acceleration simulating and control subsystem, which could simulate the acceleration magnitude up to 9 g. They used Al_2O_3-water nanofluid with volume concentrations varied from 0.07% to 0.1%. They found that the acceleration direction and magnitude had significant influences on the boiling heat transfer characteristics. Moreover, the HTC increased with increasing of the mass flow rate and the volume concentration and decreased with an increase of aspect ratio.

1.2. Numerical Simulation on Nanofluid Flow Boiling. There are quite a few methods used for nanofluid numerical simulation by researches, such as single-phase approach, mixture model approach, Eulerian model approach, VOF (volume of fluid) model approach, lattice Boltzmann method (LBM), and homogeneous two-component model [6, 7].

Sivasankaran and Mallawi [16] simulated boiling flow heat transfer of water-based copper nanofluid inside both simple pipe and aluminum metal foam pipe using the Eulerian approach. The simulated results of HTCs were compared with the Chen [17] correlation, and the value differed from the Chen correlation within ±14%. Husain et al. [18] numerically studied the low flow rate convection boiling of Al_2O_3-water nanofluids in a high aspect ratio narrow vertical annulus using a two-phase approach with the RPI wall boiling model. The contour plots of temperature, velocity, and vapor fraction were obtained, and the results showed that the maximum of average Nusselt number is at 0.5% volume concentration of nanofluids with the maximum enhancement of HTC that was 42.1%. However, when the volume concentration was larger than 0.5%, adding nanoparticles was not fruitful at all. Mohammed et al. [19] investigated the simulation on the flow boiling process of ZnO-R134a nanofluid in a horizontal tube of metal foam as a porous medium, and the mixture model was employed to analyze the variation of vapor fraction and HTC. They found that the vapor volume fraction and HTC were enhanced by 7.1% and 9.4% compared with the case of without metal foam and, also, were enhanced by 1.6% and 3.5% using the porosity of 90%. For investigating the $ZnBr_2$-acetone with graphene nanofluid flow boiling in the vapor absorption refrigeration system, Mohammed et al. [20] used the mixture model to analyze the parameters and the bubble's behavior and validated with the results of the experimental study as well. Besides, the VOF model was employed to simulate the boiling process of four miscible phases which consisted of acetone, $ZnBr_2$, graphene, and acetone vapor because the VOF was appropriate for the immiscible phases. Soleimani et al. [21] numerically researched the subcooled flow boiling of HFE-7100 containing different concentrations of alumina nanoparticles in a microchannel heat sink using the VOF model. The results indicated that the microchannel wall temperature in flow boiling was much lower than the wall temperature in single-phase flow. Also, the average microchannel wall temperature slightly decreased with an increase in nanofluid concentrations, and nanofluids with 4% volumetric concentration enhanced the heat transfer coefficient by up to 3%.

According to the above literature review, numerous researchers present the investigations on the nanofluids flow boiling heat transfer characteristic by experiment and

numerical simulation ways; however, there is only one literature conducted research on nanofluid HTC under hypergravity experimentally, and no literature studied visualization on nanofluid under hypergravity neither experimentally nor using numerical simulation method. The present study concentrates on the change of Al_2O_3-water nanofluids boiling flow patterns, which have a significant effect on the flow boiling heat transfer characteristics, in a 2 mm ID tube under different gravity levels and directions by means of numerical simulation due to the difficulty of experimental visualization for micro/minichannel. For this purpose, the VOF model approach is used for analyzing the boiling flow patterns since its superiority to predict interface motion between liquid phase and vapor phase. All the base fluid properties are considered to be temperature dependent, and the numerical predictions of water flow boiling HTCs are compared with experimental results in order to evaluate the accuracy of the numerical simulation method employed in the present research. Also, the flow boiling HTCs under different gravity levels and directions are analyzed.

2. Thermophysical Properties of Al_2O_3-Water

The thermophysical properties of nanofluids, including density ρ, specific heat capacity c_p, thermal conductivity λ, viscosity μ, and surface tension σ, have significant influence on the heat transfer behavior. Thus, study on the changes in the thermophysical properties of nanofluid and base fluid are essential before boiling flow pattern simulated in this paper.

The density and specific heat capacity of nanofluid can be estimated according to the mixture model, while the changes in thermal conductivity, viscosity, and surface tension of nanofluid are complicated. There are many researches that present the enhanced thermal conductivity as well as increased viscosity of many kinds of nanofluids in different conditions compared with base fluid. The trends of the relationship between the thermal conductivity or viscosity of nanofluid and their influence factors (temperature, particle size, and volume concentration) have been widely investigated by experiment and theoretical researches. However, the experimental data of nanofluids' thermophysical properties are insufficient, especially the description of the relationship between the thermal conductivity, viscosity, and nanoparticle size; temperature is very inconsistent. Up to now, surface tension of nanofluid has attracted less attention even if it is a very important parameter in fluid boiling. Some models of the thermal conductivity and viscosity are introduced in the present paper, and also, select the most suitable and reliable model for carrying out the following simulation work.

2.1. Density and Specific Heat Capacity. The density and specific heat capacity correlation of nanofluids are applicable to conventional fluid-solid mixtures, which are reported by Pak and Cho [22] and Buongiorno [23], respectively, as shown in Equations (1) and (2). The density, specific heat capacity, thermal conductivity, viscosity, and surface tension of base fluid water are assumed to be temperature-dependent [24, 25], as shown in Equations (3), (4), (13), (18), and (20).

$$\rho_{\mathrm{nf}} = \varphi\rho_p + (1-\varphi)\cdot\rho_f, \tag{1}$$

$$C_{P,\mathrm{nf}} = \frac{\varphi\left(\rho_p \cdot C_{P,p}\right) + (1-\varphi)\cdot\left(\rho_f C_{P,f}\right)}{\rho_f}, \tag{2}$$

$$\rho_f = 1000\left(1 - \frac{(T+273.15)+15.7914}{508928.2((T+273.15)-205.0204)}\left((T+273.15)-277.1363\right)^2\right), \tag{3}$$

$$C_{p,f} = 9616.873445 - 48.73648329T + 0.1444662T^2 - 0.000141414T^3. \tag{4}$$

2.2. Thermal Conductivity. One of the pioneering works on the thermal conductivity was conducted more than one hundred years ago by Maxwell [26], who proposed a new static model Equation (5) for predicting the thermal conductivity of fluids with multiphase.

$$\frac{\lambda_{\mathrm{nf}}}{\lambda_f} = \frac{\lambda_p + 2\lambda_f + 2\varphi\left(\lambda_p - \lambda_f\right)}{\lambda_p + 2\lambda_f - \varphi\left(\lambda_p - \lambda_f\right)}. \tag{5}$$

Based on the above model, Koo and Kleinstreuer [27] proposed a theoretical model of nanofluid's thermal conductivity in the form of Equation (6). This model takes into account the effects of Brownian motion, nanoparticle volume concentration, particle size, and temperature dependence, as well as including the properties of the base liquid.

$$\frac{\lambda_{\mathrm{nf}}}{\lambda_f} = \frac{\lambda_p + 2\lambda_f + 2\varphi\left(\lambda_p - \lambda_f\right)}{\lambda_p + 2\lambda_f - \varphi\left(\lambda_p - \lambda_f\right)} + 5\times10^4\frac{\rho_f C_{P,f}\beta\varphi}{\lambda_f}\sqrt{\frac{k_B T}{\rho_p d_p}}f(T,\varphi), \tag{6}$$

where k_B is the Boltzmann constant, the value is 1.38066×10^{-23} J/K, and for Al_2O_3-water nanofluid, β and $f(T,\varphi)$ are calculated by Equations (7) and (8), respectively.

$$\beta = \frac{8.4407}{(100\varphi)^{1.07304}}, \tag{7}$$

$$f(T,\varphi) = \left(2.8217\times10^{-2}\varphi + 3.917\times10^{-3}\right)\left(\frac{T}{T_0}\right) + \left(-3.0669\times10^{-2}\varphi - 3.91123\times10^{-3}\right). \tag{8}$$

Soon after that, Vajjha and Das [28] developed new correlations of β and $f(T,\varphi)$ of three nanofluids based on their experiment data as follows:

$$\beta = \frac{0.0017}{(100\varphi)^{0.0841}}, \tag{9}$$

$$f(T,\varphi) = (-6.04\varphi + 0.4705)T + (1722.3\varphi - 134.63). \tag{10}$$

Also, Corcione [29] proposed an empirical correlation to predict the thermal conductivity of different nanofluids (Al_2O_3, CuO, TiO_2, and Cu dispersed in water or EG) based on a large number of experimental data available in the literature, and Wang and Wu [30] concluded that the Corcione model could predict the thermal conductivity of Al_2O_3-water with the maximum deviation less than 3.87% through comparing the predicted thermal conductivities of Al_2O_3-water and experimental data from Das et al. [31, 32]. Thus, Corcione correlation as Equation (11) is used in the present paper.

$$\frac{\lambda_{\mathrm{nf}}}{\lambda_f} = 1 + 4.4\mathrm{Re}^{0.4}\mathrm{Pr}^{0.66}\left(\frac{T}{T_{\mathrm{fr}}}\right)^{10}\left(\frac{\lambda_p}{\lambda_f}\right)^{0.03}\varphi^{0.66}, \tag{11}$$

$$\mathrm{Re} = \frac{\rho_f k_B T}{\pi \mu_f^2 d_p}, \tag{12}$$

$$\lambda = -1.1245 + 0.009734T - 0.00001315T^2, \tag{13}$$

where T_{fr} is the freezing point of the base liquid.

2.3. Dynamic Viscosity. The first investigation on viscosity was done by Einstein [33]. He derived a theoretical model Equation (14) to predict the viscosity of a solid-liquid suspension for concentrations of up to 2%, but it was only applied to the suspension which was composed of milli-/micrometer scale solid particles and based fluid.

$$\frac{\mu_{\mathrm{nf}}}{\mu_f} = 1 + 2.5\varphi. \tag{14}$$

After that, many viscosity models were developed to extend Einstein's model. Nguyen et al. [34] investigated the effect of nanoparticle diameter on the viscosity of Al_2O_3-water nanofluids and developed Equation (15) by analyzing their experimental data for nanoparticle diameter of 36 nm and 47 nm.

$$\frac{\mu_{\mathrm{nf}}}{\mu_f} = 1 + 0.025\varphi + 0.015\varphi^2. \tag{15}$$

Corcione [29] also presented correlation of nanofluid dynamic viscosity as Equation (16), and the influence of temperature to the viscosity was considered as Equation (18).

$$\frac{\mu_{\mathrm{nf}}}{\mu_f} = \frac{1}{\left(1 - 34.87\left(d_p/d_f\right)^{-0.3}\varphi^{1.03}\right)}, \tag{16}$$

$$d_f = 0.1\left(\frac{6M}{N\pi\rho_f}\right)^{1/3}, \tag{17}$$

$$\mu_f = 0.02165 - 0.0001208T + 1.7184 \times 10^{-7}T^2. \tag{18}$$

Das et al. [31, 32] had done some comparison work between some viscosity models and the experimental data, and it was found that the Corcione model was the most consistent with the experiment data with deviation less than 1.03%. Therefore, Corcione correlation is chosen in the present paper for simulation.

2.4. Surface Tension. The research on the surface tension of nanofluid is scarce to be found. Sysyzkowski equation as shown in Equation (19) (Gu et al. [35]) reflected the relationship between the surface tension of nanofluid and pure water, and the experiment results from Zhu et al. [36] were used to fit the factors of a and b as $a = 7.673 \times 10^{-7}$ and $b = -7.773 \times 10^{-3}$. Das et al. [31, 32] compared the experiment data and predicted values by Equation (16), and they found the deviation was less than 4.35%. Therefore, the Sysyzkowski equation (Equation (19)) is suitable for predicting the surface tension of Al_2O_3-water nanofluid in the present research, and the influence of temperature on the surface tension of base fluid is considered as Equation (20):

$$\frac{\sigma_f - \sigma_{\mathrm{nf}}}{\sigma_f} = b\ln\left(\frac{\sigma}{a} + 1\right), \tag{19}$$

$$\sigma_f = 0.07595 - 1.47995 \times 10^{-4}T - 2.23684 \times 10^{-7}T^2. \tag{20}$$

3. Computational Method

3.1. Meshing and Independence Check for Grid. In the present study, flow boiling inside a micro/minichannel was simulated. The 2D geometry was created using the DesignModeler module in the Ansys workbench, which had length of 200 mm and ID of 2 mm. The physical dimension of the geometry model was the same as the test section in experiment, which was conducted for validating the simulation model. Then, the grid structure was generated in the Ansys mesh module, and the quadrilateral structural mesh was used so as to resolve the liquid-vapor interface accurately. The physical boundaries were defined as inlet, outlet, and walls, as shown in Figure 1. At the inlet of the tube, velocity inlet with temperature of 373.15 K was employed, and pressure-out condition was used at the outlet of the tube. The walls were regarded as static with no-slip walls, and the material was copper with thickness of 1 mm and thermal conductivity was 390 W/m K. Besides, the wall was heated by the constant heat flux of 100 kW/m^2. In addition, in order to display more reliable results, mesh was focused on near the wall side with an expand ratio of 1.2 and the layer number was 8, as depicted in Figure 2.

Because the computational accuracy increases with the amount of grid until a certain range, the grid quantity increment will also increase the computational time. Therefore, to keep a balance between the computational accuracy and time, a grid independence check was carried out before the numerical computation to find a suitable grid structure. Five kinds of grid structures with the grid quantity of 26,109, 51,149, 74,028, 122,116, and 181,998 were selected for comparison under the same computational conditions. Since the

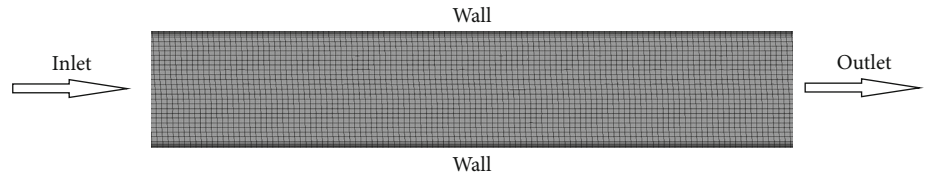

Figure 1: Schematic of grid.

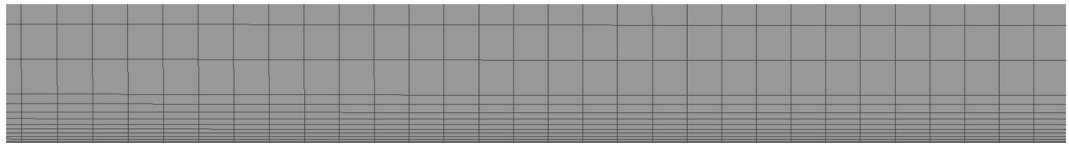

Figure 2: Local grid near the wall.

aim of the present study was to investigate the boiling flow patterns of nanofluid, the simulations on the two-phase flow of water were conducted with inlet temperature, velocity, and wall heat flux keeping at 373.15 K, 0.5 m/s, and 50 kW/m^2, respectively. The results for the wall HTC after long enough computational time were compared, as shown in Figure 3. With the increment of grid quantity, the wall HTC increases gradually, and when the grid quantity increases from 122,116 to 181,998, the wall HTC difference is only 0.1 kW/m^2 K, which indicates that the simulation results of the wall HTC are well within the asymptotic range of convergence. Therefore, the grid structure of 122,116 was selected in the present research, and the maximum size of this grid structure was limited to 0.04 mm so as to capture the more bubble formation and small nanofluid droplets.

3.2. Multiphase Model. There are two general approaches for modeling the flow of solid-liquid mixtures. For low solid volume fractions, the most suitable approach is the Lagrangian-Eulerian which analyzes the base fluid by the Eulerian assumption and the particle phase by the Lagrangian one. For higher solid volume fractions, the appropriate approach is the Eulerian-Eulerian. For nanofluids, the number of particles in the computational domain, even for a very small particle volume fraction, is extremely large due to the very small size of the particles. Therefore, this makes it impossible to solve the nanofluid flow problems by the Lagrangian-Eulerian approach due to limitations, and the Eulerian-Eulerian approach is more suitable for nanofluid simulation. There are three different Eulerian-Eulerian models, VOF, mixture, and Eulerian.

The VOF model solves a single set of momentum equations for all the phases and tracks their volume fraction all over the domain of study by solving a continuity equation for the secondary phases. The total summation of the volume fractions for all the phases is equal to unity. Therefore, the magnitude of the primary phase volume fraction will be calculated. In this method, all of the physical properties are calculated by taking a weighted average of different phases based on their volume fraction throughout each control volume. The single set of momentum equation is solved to find the velocity components, which are shared by all the phases.

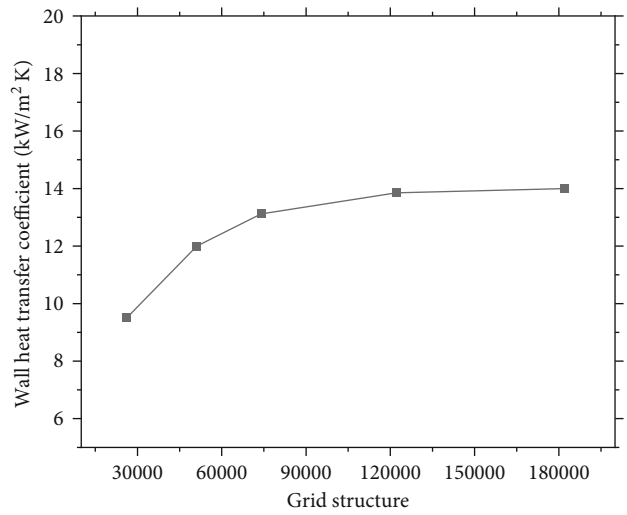

Figure 3: Grid independence study.

In the same manner, a shared temperature is calculated from a single energy equation [37]. In the present study, choose the VOF model presented by Hirt and Nichols [38] as a computational model because of the superiority in boiling flow pattern simulation.

The differential equation for conservation of mass is presented as follows:

$$\nabla \cdot \left(\varphi_q \rho_q u_q\right) = 0, \tag{21}$$

where $\Sigma_{q=1}^{n} \varphi_q = 1$ and all properties are calculated like $N = \Sigma_{q=1}^{n} \varphi_q N_q$.

In the VOF model, the momentum equation is solved for each computational cell and the resulting flow field is applied to all phases of that cell; the equation is formulated as

$$\frac{\partial}{\partial t}\left(\rho \vec{v}\right) + \nabla \cdot \left(\rho \vec{v}\vec{v}\right) = -\nabla P + \nabla \cdot \left(\mu \nabla \vec{v} + \nabla \vec{v}'\right) + \rho g + \vec{F}, \tag{22}$$

Table 1: Comparison between the simulation results and experimental data.

Inlet temperature K	Inlet velocity m/s	Wall heat flux kW/m^2	Experimental HTC kW/m^2 K	Numerical HTC kW/m^2 K	Error %
373.15	0.1	108	22.2	25.3	14
373.15	0.2	108	25.9	29.1	12.3
373.15	0.3	108	29.3	33.1	12.9
373.15	0.3	188	30.6	34.2	11.8
373.15	0.4	188	31.1	34.5	10.9
373.15	0.5	188	33.5	37.8	12.8

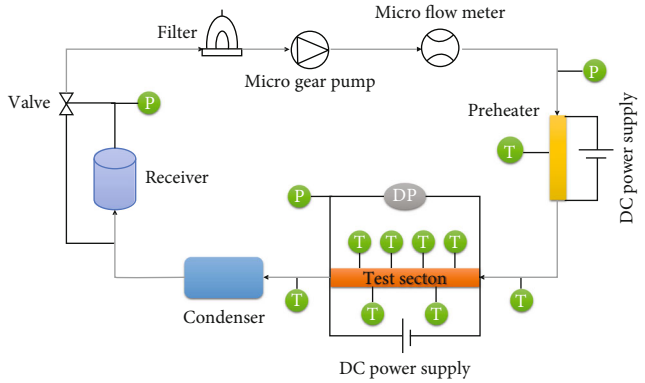

Figure 4: Schematic diagram of experimental apparatus for flow boiling loop.

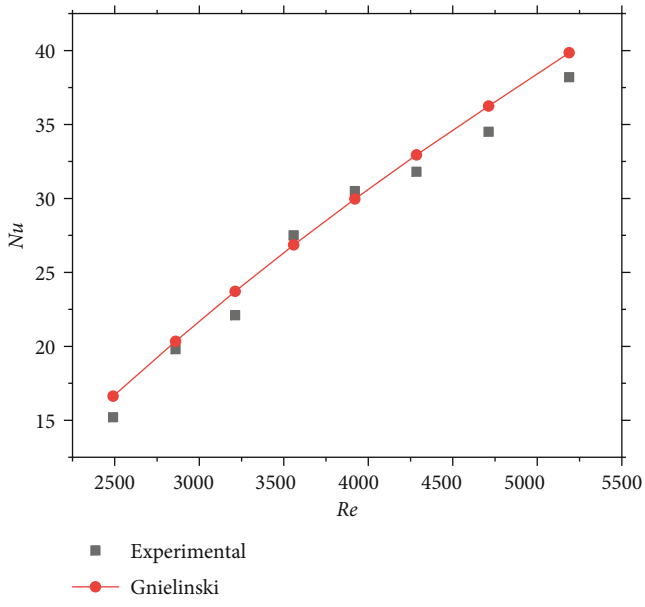

Figure 5: Comparison of the measured single-phase Nu with Gnielinski [39] prediction.

where $\vec{F}$ denotes the surface tension forces at the joint surface between two phases and P is the pressure. These forces create due to the existence of the attractive forces between molecules in a fluid. They act for balancing the radially inward intermolecular attractive force with the radially outward pressure gradient force through the interface. It should be stated that the gravity term (ρg) in the above equation has a capability for making the natural gravitational drag to condense vapor into pure water to drop out.

Table 2: Properties of water and nanoparticle (298.15 K).

Properties	Water	Al_2O_3
ρ (kg/m^3)	999.2	3950
C_p (J/kg K)	4182	765
λ (W/m K)	0.6	35
μ (Pa s)	0.001003	/

The energy equation is presented in the following form:

$$\frac{\partial}{\partial t}(\rho E)+\nabla\cdot\left(\vec{v}\,(\rho E+P)\right)=\nabla\cdot(\lambda\nabla T)+S_E, \tag{23}$$

where S_E is the energy source, which contains the radiation and any other volumetric heat sources. E is energy and can be calculated by the following relation:

$$E=\frac{\sum_{k=1}^{q}\varphi_k\rho_k E_k}{\sum_{k=1}^{q}\varphi_k\rho_k}, \tag{24}$$

where E_k for each phase is dependent on the specific heat of that phase and the temperature.

3.3. Mass and Energy Transfer Model. The physics of the boiling process consists of a mass transfer from the liquid phase to the vapor phase; thus, in this numerical model, the mass transfer is calculated using the Lee model [39]. Based on this model, mass transfer from a liquid phase to the vapor phase occurs if the temperature of the liquid is higher than the saturation temperature, and the mass transfer from the vapor phase to the liquid phase occurs if the temperature of the vapor is lower than the saturation temperature. A user-defined function (UDF) for the mass and energy source terms due to evaporation is developed using C language and leading in the Ansys Fluent software depending on Equations (25)–(27) of the Lee model.

$$S_M=-0.1\varphi_l\rho_l\left|\frac{T_l-T_{\text{sat}}}{T_{\text{sat}}}\right|, \tag{25}$$

Table 3: Boundary conditions.

Inlet velocity m/s	Wall heat flux kW/m^2	Inlet temperature K	Volume fractions vol.%	Gravity levels g
0.3	300	373.15	0.02, 0.05, 0.1	1, 1.41, 2.24, 3.16, 6, 9

$$S_M = 0.1\varphi_l\rho_l\left|\frac{T_l - T_{\text{sat}}}{T_{\text{sat}}}\right|, \quad (26)$$

$$S_E = -0.1\varphi_l\rho_l\left|\frac{T_l - T_{\text{sat}}}{T_{\text{sat}}}\right|\Delta h_{\text{lg}}, \quad (27)$$

where S_M is the mass source, h_{fg} is the enthalpy of the evaporation, and T_{sat} is saturation temperature.

3.4. Computational Methodology. Due to the standard $\kappa - \varepsilon$ model that is appropriate for boiling fluid, the standard $\kappa - \varepsilon$ turbulence model with nonequilibrium wall function is used for boiling flow pattern simulation. The solver of Fluent is pressure based with double precision. The transient solution is selected in present flow boiling simulations according to the nature of the boiling phenomenon; therefore, time step sizing is considered variable and its value is determined by courant number (Co) in Equation (28) with a fixed courant number of 0.1.

$$\text{Co} = \frac{u\Delta t}{\Delta x}, \quad (28)$$

The PISO (Pressure-Implicit with Splitting of Operators) pressure-velocity coupling method is employed for solution, and the pressure, momentum, volume fraction, and energy equations are discretized by body force weighted, QUICK (Quadratic Upstream Interpolation for Convective Kinetics), georeconstruct, and second-order upwind scheme, respectively. The underrelaxation factors of pressure, density, body force, energy, and turbulence coefficient are from 0.1 to 0.5 according to the convergence rate. The iterations are performed using the Gauss–Seidel method until all the residuals reached below 1×10^{-6}.

The percentage of the wall temperature difference at twenty consecutive previous time steps is calculated to make sure that each simulation reaches the steadiness with percentage below 1%; thus, the step is considered the steady. At low gravity levels (less than 3 g), the time step is 10^{-5}, while the time step is 10^{-6} or 10^{-7} at high gravity levels (larger than 3 g) because the flow field changes sharply. All the material properties, initial values of temperatures, pressures, velocities, and volume fraction are provided to run the simulations in Fluent.

4. Results and Discussion

4.1. Model Validation. To ensure the accuracy of the simulation results, a comparison of wall HTC was made between the simulation results and experimental data as given in Table 1. Figure 4 shows the schematic diagram of the flow boiling experimental system which consists of a receiver, a micro gear pump, a micro flow meter, a preheater, a test section, and a condenser. The working fluid was DI water, which was pumped by the micro gear pump from the receiver, firstly. After coming out of the micro gear pump, the liquid water flowed through the micro flow meter and entered the preheater, where it was heated to the saturation state with a preset vapor quality by adjusting the preheater DC supply power. Finally, the two-phase water flowed into the test section, and the wall HTCs of the test section were obtained. The test section was made of a 200 mm long straight copper tube with an inner diameter of 2.01 mm and an outer diameter of 4 mm and was wound uniformly with an enameled Ni-Cr wire with diameter of 0.3 mm as the heating device. Besides, all the tubes and containers in the flow boiling loop were well insulated, and all the tube connections had smooth interfaces to avoid the interference on the flow patterns. Six T-type thermocouples were used in the present experiment to measure the outer wall temperatures of the test section.

To verify the reliability of the experimental setup for two-phase flow boiling HTC, the experimental single-phase Nusselt number was compared with the Gnielinski [40] correlation. The validation is illustrated in Figure 5, which shows the well agreement between the prediction and experimental results, indicating that the experimental setup for flow boiling heat transfer is reliable.

From Table 1, it can be seen that the results achieved by numerical simulation perform good agreement with the experimental data with a maximum error of 14%. It should be noted that there is always a deviation between the numerical results and experimental results due to the errors which come from the experimental factors and computational factors. The experimental factors contain experiment accuracy, calibration for measurements, human errors, etc. The computational errors created by some simplification assumptions such as two-dimensional modeling, and the walls are adiabatic in this numerical modeling, while they are not completely adiabatic in the experiments.

4.2. Conditions for Simulation. The thermophysical properties of the basic fluid water and nanoparticle Al_2O_3 are illustrated in Table 2, and the boundary conditions are inlet velocity of 0.3 m/s, inlet temperature of 373.15 K, wall heat flux of 300 kW/m^2, volume fraction of 0.02%, 0.05%, and 0.1%, and gravity levels from 1 g to 9 g, as shown in Table 3. Some gravity level values are 1.41 g, 2.24 g, and 3.16 g on account of the centrifugal experimental apparatus in the author's lab refer to Li et al. [2, 4]. At downward perpendicular to flow direction, same as flow direction, and opposite to flow direction, the volume fractions of 0.02%, 0.05%, and 0.1% nanofluids are used as working fluid for simulation, respectively.

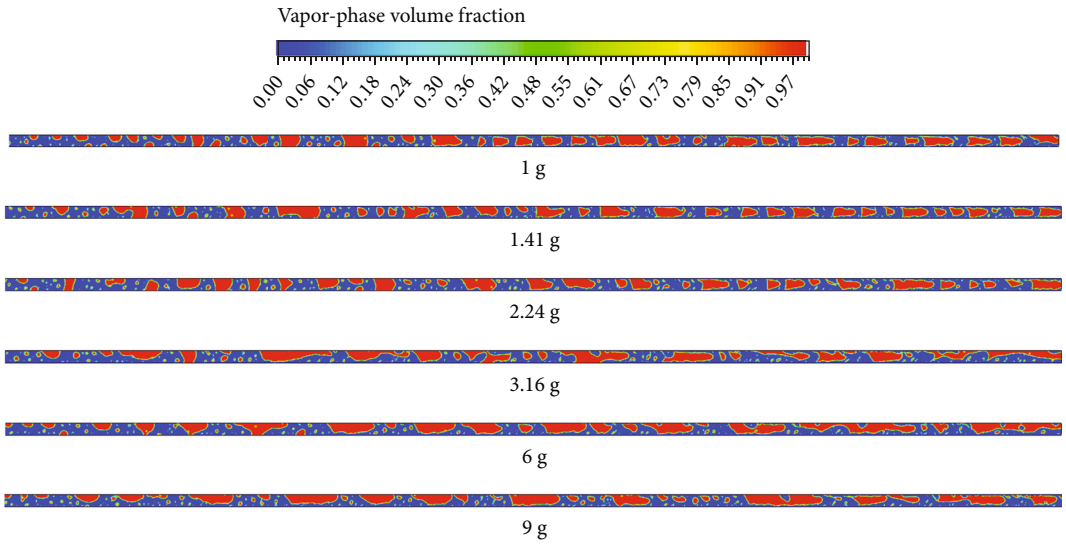

Figure 6: Diagram of boiling flow patterns of 0.02% nanofluid at gravity levels from 1 g to 9 g (The gravity direction is downward perpendicular to the flow direction).

4.3. Perpendicular to the Flow Direction Results. Figure 6 shows the changing of vapor phase volume fractions (boiling flow patterns) during different gravity levels from 1 g to 9 g, and the working fluid, which is 0.02% nanofluid, flows from left to right; the gravity directions are downward perpendicular to the flow directions. With the computational time steps go on, the vapor is visible and quickly increases near the walls, then, gathers there and becomes a large bubble till that forms a vapor plug. During the gathering of the vapor phase at the walls, the vapor phase moves faster than the other phase toward the exit. Therefore, the trends of flow patterns are bubbly flow, plug flow, slug flow, and wavy flow. From Figures 6(a)–6(f), it can be seen that hypergravity has a significant effect on all kinds of flow patterns. With the increment of gravity levels, the flow patterns will evolve into stratified flow eventually. It is mainly because the buoyancy of the vapor phase increases with the increasing gravity levels; thus, the vapor phase (bubbles, vapor-plugs, and vapor-slugs) approaches to the upper wall of the tube. Moreover, the vapor phase is also affected by the inertia force and viscous force at the same time, which leads to the bubbles becoming slenderer and longer gradually. Finally, the flow patterns transform to stratified flow because of combining of bubbles with each other.

The wall heat transfer coefficient is also analyzed and displayed in Figure 7. Along the tube wall from inlet to outlet, the HTC increases with the increasing of vapor quality. Near the inlet of the tube, the flow pattern is bubbly flow with low vapor quality, so the HTC is lower than 10 kW/m^2 K, and the influence of hypergravity is inapparent on the HTC. With the vapor quality increasing, the bubbles gather and transform to the vapor-plug and vapor-slug; thus, the transformation of flow pattern results in the change of HTC is not significant at the middle section of the tube when the gravity levels are less than 3 g. When the gravity levels are greater than 3 g, the buoyancy increases gradually which results in the vapor phase gathering to the upper wall of the

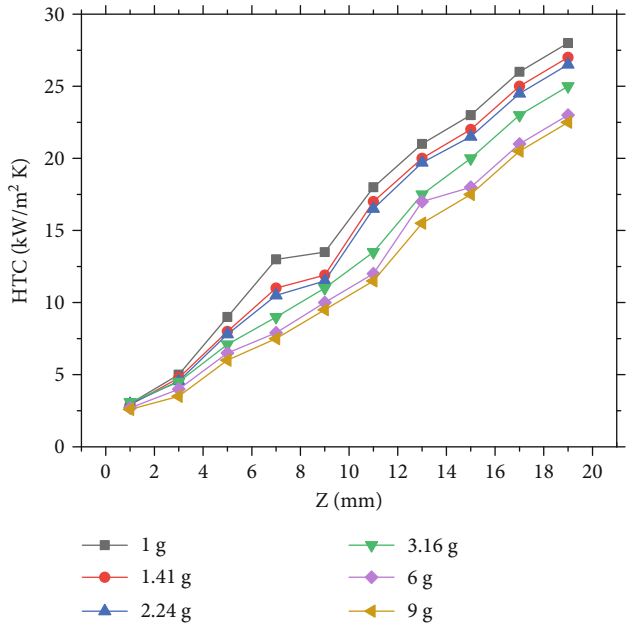

Figure 7: Heat transfer coefficient of 0.02% nanofluid under hypergravity.

tube, and vapor plug is not full of the tube. Therefore, the HTCs increase continuously from low vapor quality to high vapor quality under gravity levels that are greater than 3 g. In addition, it can be seen from Figure 7 that with the increment of gravity levels, the trends of HTC variation are more and more reduced because of the asymmetric distribution of vapor phase in tube. The maximum value of HTC is that under Earth's gravity, and the average wall HTC of 9 g has 24% reduction compared to that of 1 g. Dong et al. [1] tested flow boiling heat transfer of Al_2O_3-water nanofluids in swirl microchannels under gravity levels up to 9 g, and they also found that the HTC reduced with an increase of the acceleration magnitude. They considered the main reason was that

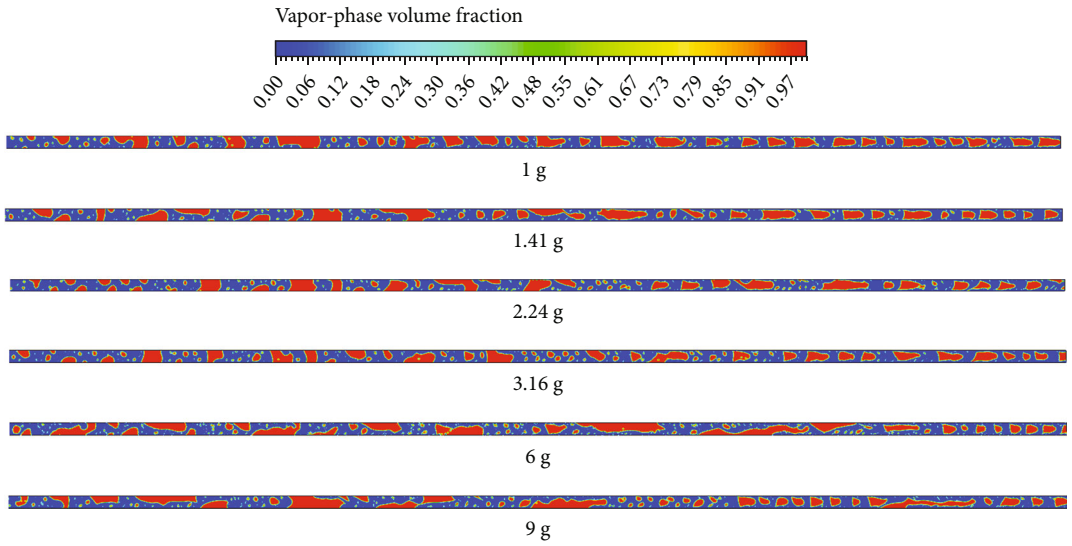

Figure 8: Diagram of boiling flow patterns of 0.05% nanofluid at gravity levels from 1 g to 9 g (The gravity direction is the same as the flow direction).

the higher acceleration magnitude led to an increase of the local wall temperature; thus, the heat transfer performance was deteriorated.

4.4. Same as the Flow Direction Results. The changes of flow patterns under hypergravity when gravity direction is the same as the flow direction are depicted in Figure 8. Apparently, hypergravity also has influence on the flow patterns in this situation but the results are different from that the gravity direction is perpendicular to flow direction. When the gravity level is lower than 3.16 g, the changes of flow patterns are not significant while the changes are distinct at 6 g and 9 g. From Figures 8(e) and 8(f), it can be seen that most vapor plugs are not filled with the tube and unobstructed compared to that at lower hypergravity. Moreover, at the second half of the tube, the vapor slugs become shorter and more and more circular with the increasing of gravity levels. The primary reason is that the influence of inertia force enhances while the viscous force is getting weaker and weaker during the increment of the gravity levels, which results the vapor plugs do not block up the tube and the shape of vapor slugs becomes round by degrees. Also, some vapor slugs are elongated by the influence of inertia force under high gravity levels, as shown in Figures 8(e) and 8(f).

The effect of hypergravity on the HTCs of 0.05% nanofluid is illustrated in Figure 9. The HTCs along the tube wall show the similar trends to the 0.02% nanofluid's HTC case, namely, increase with the increasing of vapor quality from inlet to outlet. Moreover, the wall HTC is decreasing with the increasing of the gravity levels, and the main difference from the 0.02% nanofluid's case is that the wall HTC of the second half of the tube is affected by hypergravity significantly, while the effect on the first half of the tube is slightly due to the difference of flow patterns as shown in Figure 6. At the slug flow period, the vapor slug is shorter and shorter because of the increasing of the inertia force and decreasing of the viscous force with the gravity levels increasing; therefore, the value of wall HTC shows the reduced trend along with the increment of hypergravity.

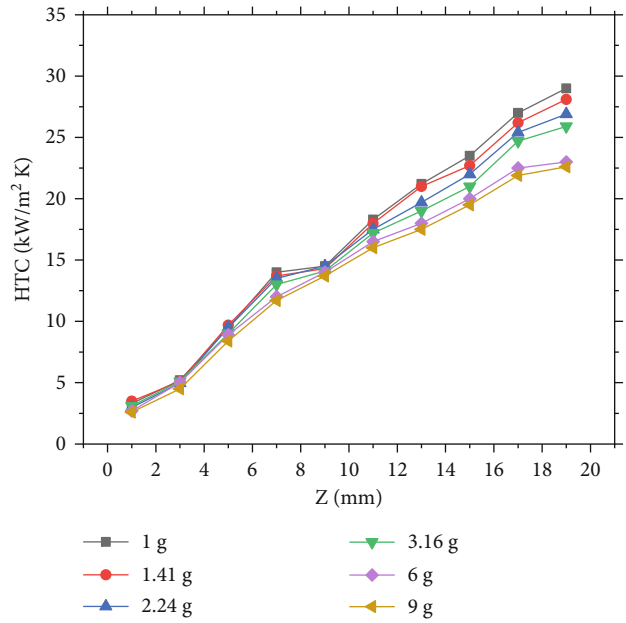

Figure 9: Heat transfer coefficient of 0.05% nanofluid under hypergravity.

4.5. Opposite to the Flow Direction Results. When the gravity direction is opposite to the flow direction, the influence of hypergravity on the flow patterns is illustrated in Figure 10. Obviously, the results are contrary to that at gravity direction is the same as flow direction. It can be seen that for the bubbly flow, the influence of hypergravity is inconspicuous, while for the plug flow and slug flow, the vapor phase is elongated by the combined effect of inertia force and viscous force because of the decreasing of inertia force

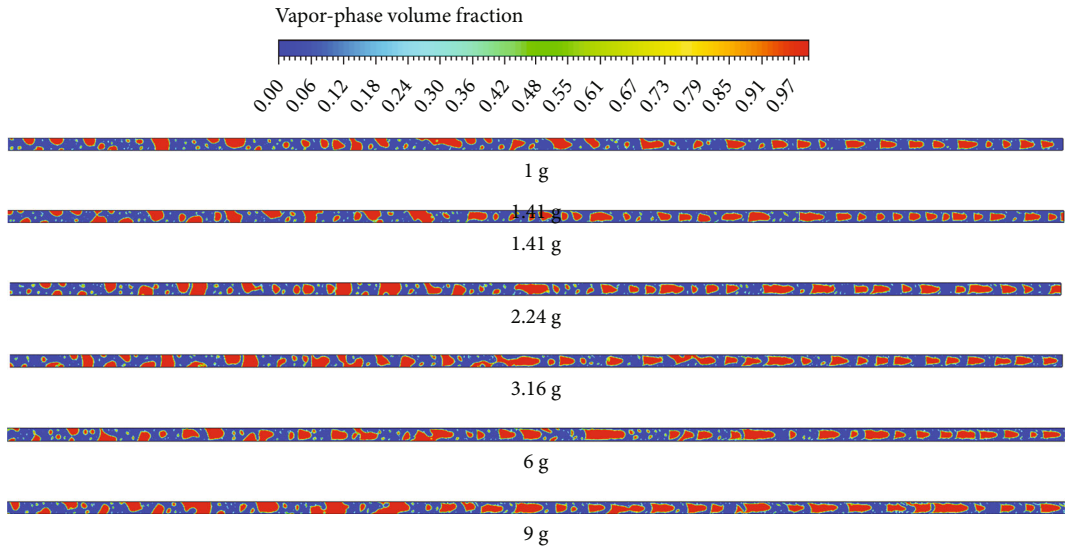

Figure 10: Diagram of boiling flow patterns of 0.1% nanofluid at gravity levels from 1 g to 9 g (The gravity direction is opposite to the flow direction).

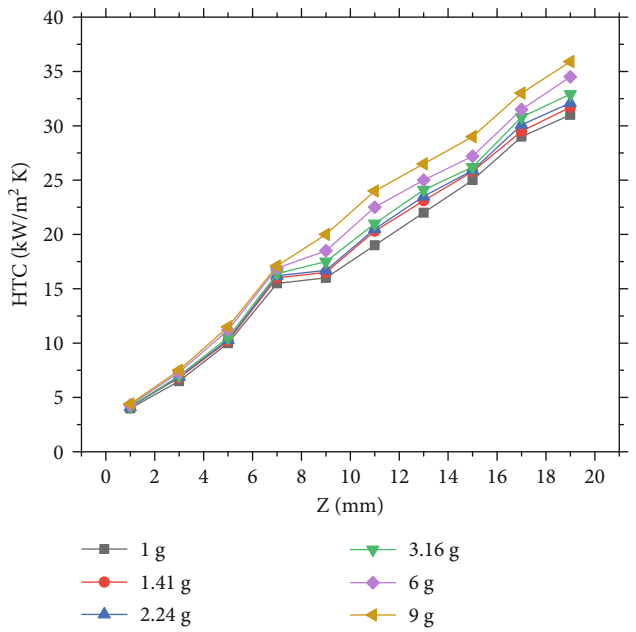

Figure 11: Heat transfer coefficient of 0.1% nanofluid under hypergravity.

and increasing of viscous force with increment of gravity levels. Also, the flow patterns of 1 g to 3.16 g are similar to each other, and the flow patterns have obvious variety till 6 g. Consequently, a higher gravity level is needed for future experiment.

Figure 11 illustrates the numerical results of 0.1% nanofluid's wall HTC under gravity levels from 1 g to 9 g, and the gravity direction is contrary to the flow direction. Compare Figure 11 with Figures 6 and 8, there is a big difference between the 0.1% nanofluid case and other two cases that with the gravity levels increasing, the second half of the tube's wall HTC shows the enhanced tendency. Near the outlet, the value of HTC at 9 g is more than 20% higher than the HTC at Earth's gravity. This is mainly because the larger traction by viscous force at a higher gravity level causes the vapor slug to elongate; hence, the velocity between the liquid film and inner wall surface increases, which in turn causes the increment of wall HTC.

5. Conclusions

In the present study, analyze the density ρ, specific heat capacity c_p, thermal conductivity λ, viscosity μ, and surface tension σ of nanofluids at first, and chose the most suitable theoretical model of λ, μ, and σ for simulations. The grid structure of 122,116 was selected after grid independence check. The model validation was made by comparing the wall HTC of between the simulation results and experimental data. Then, a series of simulations on the boiling flow patterns of Al_2O_3-water nanofluid in a 2 mm tube under hypergravity were conducted, with three different gravity directions (perpendicular to flow direction, same as flow direction, and opposite to flow direction) from 1 g to 9 g. Four kinds of flow patterns, including bubbly flow, plug flow, slug flow, and wavy flow were gained to investigate the influence of hypergravity on the flow patterns. Some conclusions are summarized in the following:

(1) When hypergravity direction is perpendicular to the flow direction, the vapor phase (bubbles, vapor-plugs, and vapor-slugs) approaches to the upper wall of the tube due to the effect of buoyancy, then, becomes slenderer and longer with the gravity levels increasing, and transforms to the stratified flow at last. The trends of wall HTC variation show reduction with the increment of hypergravity because of the asymmetric distribution of vapor phase in tube

(2) The vapor phase transforms to short circular gradually with increasing of hypergravity when hypergravity direction is the same as the flow direction. The main reason is that the inertia force is increasing with the gravity levels increasing, and the shear force is decreasing at the same time. The wall HTC of the second half of the tube is affected by hypergravity significantly, while the effect on the first half of the tube is slightly, and decreasing with the increasing of the gravity levels

(3) On the contrary, vapor phase becomes elongated when the hypergravity direction is opposite to the flow direction due to the decreasing of inertia force and increasing of shear force. The influence of hypergravity for the bubbly flow is slight but is significant for the plug flow and slug flow. The second half of the tube's wall HTC increases with the increasing of hypergravity, and the value is more than 20% higher at 9 g than that at 1 g near the outlet

The boiling flow patterns of nanofluid under different gravity levels and directions shown in the present study can provide useful guidance for future study and design of nanofluid-based heat exchangers in aircraft. As is known that the thermophysical properties of nanofluid have a significant effect on the flow boiling characteristic, and further investigations to explore the influence of density, specific heat capacity, thermal conductivity, viscosity, and surface tension on the flow patterns will be carried out in our future study. In addition, the experimental investigations on the HTC of nanofluid flow boiling under different gravity directions will be conducted by using a centrifugal machine reported by Fang's team [2, 4, 41] to compare the HTC results in the present research.

Nomenclature

C: Specific heat capacity (J/kg K)
d: Diameter (m)
g: Earth's gravity (m/s^2)
h: Enthalpy (J/kg), heat transfer coefficient (kW/m^2 K)
P: Pressure (Pa)
Pr: Prandtl number
Re: Reynolds number
S: Source term
T: Temperature (K)
u: Velocity (m/s).

Greek Symbols

λ: Thermal conductivity (W/m K)
σ: Surface tension (N/m)
ρ: Density (kg/m^3)
φ: Volume fraction (vol.%)
μ: Dynamic viscosity (kg/m s).

Subscripts

B: Boltzmann
E: Energy
f: Fluid
fr: Standard of freezing point
l: Liquid
lg: Evaporation
nf: Nanofluid
p: Nanoparticle
sat: Saturation temperature.

Data Availability

There are no data results.

Conflicts of Interest

The authors declare that they have no known competing financial interests or personal relationships that could have appeared to influence the work reported in this paper.

Acknowledgments

This study is supported by the National Natural Science Foundation of China (52076107 and 51576099) and the Priority Academic Program Development of Jiangsu Higher Education Institutions.

References

[1] S. Dong, H. Jiang, Y. Xie, X. Wang, Z. Hu, and J. Wang, "Experimental investigation on boiling heat transfer characteristics of Al_2O_3-water nanofluids in swirl microchannels subjected to an acceleration force," *Chinese Journal of Aeronautics*, vol. 32, no. 5, pp. 1136–1144, 2019.

[2] G. Li, X. Fang, D. Tang, Z. Luo, and Y. Chen, "Étude experimentale du transfert de chaleur par ebullition en ecoulement sature du R1234yf dans un tube horizontal de 2,01 mm sous hypergravite," *International Journal of Refrigeration*, vol. 127, pp. 12–20, 2021.

[3] M. C. Vlachou, J. S. Lioumbas, M. Kostoglou et al., "Subcooled flow boiling in horizontal and vertical macro-channel under Earth- gravity and hyper-gravity conditions," *International Journal of Heat and Mass Transfer*, vol. 133, pp. 36–51, 2019.

[4] G. Li, X. Fang, Y. Yuan, Y. Chen, L. Wang, and Y. Xu, "An experimental study of flow boiling frictional pressure drop of R134a in a horizontal 1.002 mm tube under hypergravity," *International Journal of Heat and Mass Transfer*, vol. 118, pp. 247–256, 2018.

[5] S. Choi, "Enhancing thermal conductivity of fluids with nanoparticles," *ASME Publ. Fed.*, vol. 231, pp. 99–106, 1995.

[6] O. Mahian, L. Kolsi, M. Amani et al., "Recent advances in modeling and simulation of nanofluid flows-part I: fundamentals and theory," *Physics Reports*, vol. 790, pp. 1–48, 2019.

[7] O. Mahian, L. Kolsi, M. Amani et al., "Recent advances in modeling and simulation of nanofluid flows–part II: applications," *Physics Reports*, vol. 791, pp. 1–59, 2019.

[8] S. Chakraborty and P. K. Panigrahi, "Stability of nanofluid: a review," *Applied Thermal Engineering*, vol. 174, article 115259, 2020.

[9] B. Bakthavatchalam, K. Habib, R. Saidur, B. B. Saha, and K. Irshad, "Comprehensive study on nanofluid and ionanofluid for heat transfer enhancement: a review on current and

future perspective," *Journal of Molecular Liquids*, vol. 305, article 112787, 2020.

[10] K. Farhana, K. Kadirgama, M. M. Rahman et al., "Significance of alumina in nanofluid technology," *Journal of Thermal Analysis and Calorimetry*, vol. 138, no. 2, pp. 1107–1126, 2019.

[11] M. M. Sarafraz, I. Tlili, Z. Tian, A. R. Khan, and M. R. Safaei, "Thermal analysis and thermo-hydraulic characteristics of zirconia–water nanofluid under a convective boiling regime," *Journal of Thermal Analysis and Calorimetry*, vol. 139, pp. 2413–2422, 2019.

[12] M. Goodarzi, I. Tlili, H. Moria et al., "Boiling heat transfer characteristics of graphene oxide nanoplatelets nano- suspensions of water-perfluorohexane (C_6F_{14}) and water-n-pentane," *Alexandria Engineering Journal*, vol. 59, no. 6, pp. 4511–4521, 2020.

[13] M. Dadhich, O. S. Prajapati, and V. Sharma, "Investigation of boiling heat transfer of titania nanofluid flowing through horizontal tube and optimization of results utilizing the desirability function approach," *Powder Technology*, vol. 378, pp. 104–123, 2021.

[14] S. Mukherjee, S. Jana, P. Chandra Mishra, P. Chaudhuri, and S. Chakrabarty, "Experimental investigation on thermo-physical properties and subcooled flow boiling performance of Al_2O_3/water nanofluids in a horizontal tube," *International Journal of Thermal Sciences*, vol. 159, article 106581, 2021.

[15] N. Patra, P. Ghosh, R. S. Singh, and A. Nayak, "Flow visualization in dilute oxide based nanofluid boiling," *International Journal of Heat and Mass Transfer*, vol. 135, pp. 331–344, 2019.

[16] S. Sivasankaran and F. O. M. Mallawi, "Numerical study on convective flow boiling of nanoliquid inside a pipe filling with aluminum metal foam by two-phase model," *Case Studies in Thermal Engineering*, vol. 26, article 101095, 2021.

[17] C. J. Chen, "Correlation for boiling heat transfer to saturated fluids in convective flow," *Industrial & Engineering Chemistry Process Design and Development*, vol. 5, no. 3, pp. 322–329, 1966.

[18] S. Husain, S. A. Khan, and M. A. Siddiqui, "Wall boiling of Al_2O_3-water nanofluid: effect of nanoparticle concentration," *Progress in Nuclear Energy*, vol. 133, article 103614, 2021.

[19] H. I. Mohammed, P. T. Sardari, and D. Giddings, "Multiphase flow and boiling heat transfer modelling of nanofluids in horizontal tubes embedded in a metal foam," *International Journal of Thermal Sciences*, vol. 146, article 106099, 2019.

[20] H. I. Mohammed, D. Giddings, G. S. Walker, P. Talebizadehsardari, and J. M. Mahdi, "Thermal behaviour of the flow boiling of a complex nanofluid in a rectangular channel: an experimental and numerical study," *International Communications in Heat and Mass Transfer*, vol. 117, article 104773, 2020.

[21] A. Soleimani, A. Sattari, and P. Hanafizadeh, "Thermal analysis of a microchannel heat sink cooled by two-phase flow boiling of Al_2O_3 HFE-7100 nanofluid," *Thermal Science and Engineering Progress*, vol. 10, article 100693, 2020.

[22] B. C. Pak and Y. I. Cho, "Hydrodynamic and heat transfer study of dispersed fluids with submicron metallic oxide particles," *Experimental Heat Transfer*, vol. 11, no. 2, pp. 151–170, 1998.

[23] J. Buongiorno, "Convective transport in nanofluids," *Journal of Heat Transfer*, vol. 128, no. 3, pp. 240–250, 2006.

[24] W. Minkowycz, E. M. Sparrow, and J. P. Abraham, *Nanoparticle Heat Transfer and Fluid Flow*, CRC press, 2012.

[25] Y. Feng and C. Kleinstreuer, "Nanofluid convective heat transfer in a parallel-disk system," *International Journal of Heat and Mass Transfer*, vol. 53, no. 21-22, pp. 4619–4628, 2010.

[26] J. C. Maxwell, *A Treatise on Electricity and Magnetism*, Clarendon press, Oxford, UK, 1881.

[27] J. Koo and C. Kleinstreuer, "A new thermal conductivity model for nanofluids," *Journal of Nanoparticle Research*, vol. 6, no. 6, pp. 577–588, 2004.

[28] S. Vajjha and D. Das, "Experimental determination of thermal conductivity of three nanofluids and development of new correlations," *International Journal of Heat and Mass Transfer*, vol. 52, no. 21-22, pp. 4675–4682, 2009.

[29] M. Corcione, "Empirical correlating equations for predicting the effective thermal conductivity and dynamic viscosity of nanofluids," *Energy Conversion and Management*, vol. 52, no. 1, pp. 789–793, 2011.

[30] Y. Wang and J. Wu, "Numerical simulation on single bubble behavior during Al_2O_3/H_2O nanofluids flow boiling using moving particle simi-implicit method," *Progress in Nuclear Energy*, vol. 85, pp. 130–139, 2015.

[31] S. Das, N. Putra, and W. Roetzel, "Pool boiling characteristics of nano-fluids," *International Journal of Heat and Mass Transfer*, vol. 46, no. 5, pp. 851–862, 2003.

[32] S. Das, N. Putra, P. Thiesen, and W. Roetzel, "Temperature dependence of thermal conductivity enhancement for nanofluids," *Journal of Heat Transfer*, vol. 125, no. 4, pp. 567–574, 2003.

[33] A. Einstein, *Investigation on the Theory of Brownian Movement*, Dover Publications, New York, 1956.

[34] C. Nguyen, F. Desgranges, G. Roy et al., "Temperature and particle-size dependent viscosity data for water-based nanofluids - hysteresis phenomenon," *International Journal of Heat and Fluid Flow*, vol. 28, no. 6, pp. 1492–1506, 2007.

[35] T. Gu, B. Zhu, and W. Li, *Surface Chemistry*, Beijing Science Press, 2004.

[36] D. Zhu, S. Wu, and N. Wang, "Surface tension and viscosity of aluminum oxide nanofluids," *AIP Conference Proceedings*, vol. 1207, pp. 460–464, 2010.

[37] M. Akbari, N. Galanis, and A. Behzadmehr, "Comparative analysis of single and two-phase models for CFD studies of nanofluid heat transfer," *International Journal of Thermal Sciences*, vol. 50, no. 8, pp. 1343–1354, 2011.

[38] C. W. Hirt and B. D. Nichols, "Volume of fluid (VOF) method for the dynamics of free boundaries," *Journal of Computational Physics*, vol. 39, no. 1, pp. 201–225, 1981.

[39] W. Lee, *A pressure iteration scheme for two-phase modeling*, Los Alamos Scientific Laboratory, Technical Report, LA-UR, Los Alamos, New Mexico, 1979.

[40] V. Gnielinski, "New equations for heat and mass transfer in turbulent pipe and channel flow," *International Chemical Engineering*, vol. 16, pp. 359–368, 1976.

[41] Y. Xu, X. Fang, G. Li, and D. Li, "An experimental investigation of flow boiling heat transfer and pressure drop of R134a in a horizontal 2.168 mm tube under hypergravity. Part II: heat transfer coefficient," *International Journal of Heat and Mass Transfer*, vol. 80, pp. 597–604, 2015.